COBEM 2023 27TH INTERNATIONAL CONGRESS OF MECHANICAL ENGENEERING

ABCM Brazilian Society of Mechanical Sciences and Engineering
27th ABCM International Congress of Mechanical Engineering
December 04-08, 2023, Florianópolis-SC, Brazil

COB-2023-1159
EFFECTS OF FREESTREAM FLOW CONDITIONS ON THE CONVERGENCE HISTORY FOR TRANSITIONAL FLOW SIMULATIONS

Aline Roberta Santos Righi
Instituto Tecnológico de Aeronáutica, 12228-903 São José dos Campos, Brazil
alinerighi29@gmail.com

Gustavo Luiz Olichevis Halila
Instituto de Aeronáutica e Espaço, 12228-904 São José dos Campos, Brazil
gustavohalila@gmail.com

João Luiz F. Azevedo
Instituto de Aeronáutica e Espaço, 12228-904 São José dos Campos, Brazil
joaoluiz.azevedo@gmail.com

Abstract. *The appropriate treatment of transition to turbulence remains a central challenge in Computational Fluid Dynamics (CFD). Although CFD simulations have been used in the design and development processes in the aerospace industry for quite some time now, the correct treatment of transitional flows over general configurations still needs some attention. The present work addresses the impact of mesh size and physical reference parameters in the residues convergence and transition front location, when considering high Reynolds number, transitional flows. The approach adopted here uses a Reynolds-averaged Navier-Stokes formulation, with the Shear Stress Transport (SST) model for turbulence closure, which is further coupled to the Langtry-Menter transition model. The SST turbulence model uses two equations of transport for turbulence closure, and the Langtry-Menter transition model uses two additional transport equations to predict the laminar-turbulent transition. The Langtry-Menter model is compatible with modern CFD techniques, such as unstructured grids and parallel processing. One main feature of transitional flows is that transition can be caused by a few different mechanisms. For example, transition can be triggered due to the amplification of Tollmien-Schlichting waves or bypass transition, and the Langtry-Menter transition model is capable of predicting both. In order to achieve the goals of the present work, the Langtry-Menter transition model is implemented in a local code that has been developed over the past years, called BRU3D. Two test cases are presented in this paper, a zero pressure gradient flat plate and the NLF(1)-0416 airfoil. For the flat plate, two different meshes, one coarse and one fine, are used in the simulations. For the NLF(1)-0416 airfoil geometry three meshes are used, one coarse, one fine, and one super fine. Also, the skin friction coefficient, c_f, is used here for all cases in order to visualize the influence over the transition location due to the mesh size and physical reference values.*

Keywords: *CFD, Laminar-Turbulent Transition, Langtry-Menter Model, Numerical Convergence.*

1. INTRODUCTION

For quite some time now, Computational Fluid Dynamic (CFD) techniques have been used in the design and development processes in the aerospace industry to treat transitional flows. Despite of that, the laminar-turbulent modeling still requires some special attention (Slotnick *et al.*, 2014). Transition phenomena play an important role in different engineering aplications, for example, in the aerodynamics of airplanes. For instance, the laminar-turbulent modeling prediction is a relevant topic in CFD given that transitional effects directly impact the drag coefficient which is essential to airplane performance estimates (Halila *et al.*, 2016, 2018). In the laminar-turbulent transition, the laminar boundary layer is excited by external factors through a mechanism called receptivity. The most common transition mechanisms for aerospace applications are the amplification of Tollmien-Schlichting (TS) waves (Klebanoff *et al.*, 1962), bypass transition (Ghasemi *et al.*, October, 2014), crossflow vortices (Saric and Dagenhart, 1999), leading edge transition and flow contamination (Poll, 1978).

Many transition modeling strategies are available in the literature to deal with transitional flows. Some of these methods can be coupled to the Reynolds-averaged Navier Stokes (RANS) equations, together with the appropriate turbulence closure models. Therefore, these models allow accurate and inexpensive transition flow predictions, with a standard, fully-turbulent RANS model with one or two transport equations based only on local parameters and empirical correlations. One of these methods is the Langtry-Menter transition model (Langtry and Menter, 2009) (LCTM - Local Correlation-based Transition Model). In the present work, the Langtry-Menter transition model is coupled to the Shear Stress Transport

(SST) (Menter, 1994) model for turbulence closure. The Langtry-Menter transition model has two additional transport equations, one for the intermittency and one for the transition momentum thickness Reynolds number.

In the past years, many studies have been conducted in order to understand not only the transition phenomena, but also the influence of the additional physical and numerical parameters on the transition location and numerical convergence history. Therefore, the Langtry-Menter transition model has been implemented in an in-house CFD code, BRU3D (Bigarella, 2007; Bigarella and Azevedo, 2009; Carvalho *et al.*, 2018), and the BRU3D code is used for all of our simulations presented here. The present paper discusses the results of a study for some reference parameters in the transition location and numerical convergence history. In order to achieve this, the flow over a zero pressure gradient flat plate, the T3A and T3B test cases, and the NLF(1)-0416 airfoil are studied.

2. THEORETICAL AND NUMERICAL FORMULATION

This section introduces the necessary numerical formulation for the present work. The formulations presented here are implemented in an in-house code, BRU3D, which is presented in the next subsection 2.1. Subsection 2.2 introduces the equations for the Langtry-Menter transition model, which is in its original formulation and can predict transition due to the amplification of Tollmien-Schilichting waves and bypass transition.

2.1 The BRU3D Code

The BRU3D code has been used for the development of this work (Bigarella, 2007; Carvalho, 2018). The BRU3D code was created and has been improved by the research group over the past years. At this point, the code can solve the Euler compressible equations and the Reynolds-averaged Navier-Stokes equations. Different turbulence models are implemented, including the Spalart-Allmaras (Spalart and Allmaras, 1994) and the Shear Stress Transport (Menter, 1994) turbulence models. An extensive validation of the code shows results in good agreement with experimental data and can be found in Bigarella (2007). Recently, the standard Langtry-Menter model, which is based on the SST turbulence model, was implemented (Carvalho *et al.*, 2018).

The BRU3D code solves the equations in a standard, cell-centered, finite volume method for general unstructured grids and can be executed using parallel MPI cells. The Roe approximate Riemann solver (Roe, 1981) is used for the calculation of numerical fluxes associated with the inviscid terms at cell interfaces. The Generalized Minimal Residual Methods (GMRES) solver is used to find numerical solution. A point-implicit time integration scheme, based on the first-order backward Euler method, is used for the temporal discretization of the governing equations and it contributes to achieve better numerical robustness (Bigarella and Azevedo, 2009).

2.2 Formulation of the Standard Langtry-Menter Transition Model

The Langtry-Menter $\gamma - Re_\theta$ transition model (Langtry and Menter, 2009) is composed of two equations in addition to the equations of the SST model (Menter, 1994). The model is based only on local variables and is compatible with modern CFD codes. In the Langtry-Menter model, the strain rate Reynolds number, which is a local variable, maps the transition momentum-thickness Reynolds number, which is nonlocal and plays an important role in transition prediction. The first transport equation of the Langtry-Menter model is for the intermittency, γ, which is used to trigger the SST source terms and represents the probability of a fluid cell to be turbulent. It is given by

$$\frac{\partial(\rho\gamma)}{\partial t} + \frac{\partial(\rho u_j \gamma)}{\partial x_j} = P_\gamma - E_\gamma + \frac{\partial}{\partial x_j}\left[(\mu + \frac{\mu_t}{\sigma_f})\frac{\partial \gamma}{\partial x_j}\right], \tag{1}$$

where ρ is the density, u_j represents the velocity vector components, P_γ is the intermittency source term, E_γ is the destruction-relaminarization source, μ is the molecular dynamic viscosity, μ_t is the eddy viscosity, and $\sigma_f = 1.0$. The complete expressions for the remaining terms can be found in Langtry and Menter (2009). The second transport equation represents the transition momentum thickness Reynolds number, $\tilde{Re}_{\theta_t}$, and is given by

$$\frac{\partial(\rho\tilde{Re}_{\theta_t})}{\partial} + \frac{\partial(\rho u_j \tilde{Re}_{\theta_t})}{\partial x_j} = P_{\theta_t} + \frac{\partial}{\partial x_j}\left[\sigma_{\theta_t}(\mu + \mu_t)\frac{\partial \tilde{Re}_{\theta_t}}{\partial x_j}\right], \tag{2}$$

where P_{θ_t} is the source term, and $\sigma_{\theta_t} = 2.0$ controls the diffusion coefficient. The transition momentum-thickness Reynolds number represents a sensor responsible for triggering the transition process, because $\tilde{Re}_{\theta_t}$ indicates the point where transition begins. The Langtry-Menter model couples the intermittency function with the SST model to activate the turbulent kinetic energy production term. The coupling takes place through the production term $\tilde{P}_\gamma$,

$$\frac{\partial(\rho k)}{\partial t} + \frac{\partial(\rho u_j k)}{\partial x_j} = \tilde{P}_k - \tilde{D}_k + \frac{\partial}{\partial x_j}\left[(\mu + \sigma_k \mu_t)\frac{\partial k}{\partial x_j}\right], \tag{3}$$

$$\tilde{P}_k = \gamma_{eff} P_k, \tag{4}$$

where $\tilde{P}_k$ and $\tilde{D}_k$ are the original production and destruction terms of the SST model, and $\gamma_{eff} P_k$ includes the separation effects in the formulation. The original formulation of the Langtry-Menter transition model is able to predict Tollmien-Schlichting waves and bypass transition mechanisms. Further information and the empirical correlations can be found in the literature (Langtry and Menter, 2009).

3. RESULTS

In the present work, two different test cases are studied and addressed for the laminar-turbulent transition, the zero pressure flat plate and the NLF(1)-0416 airfoil test cases. The test cases aim at observing the impacts in the convergence for the L-infinity norm and in the transition location through the skin friction coefficient, c_f, curves. In order to do that, different physical and numerical parameters were chosen, for instance, mesh size, number of iterations, the reference Reynolds number, the reference freestream turbulence intensity, and the reference viscosity ratio.

3.1 Flat Plate Test Case

Two test cases for zero-pressure gradient flat plates (Rumsey and Lee-Rausch, 2015; Coder, 2018) accounting for bypass transition are addressed. The reference freestream values used in the test cases are based on the experiments available in the European Research Community on Flow, Turbulence and Combustion (ERCOFTAC) website for the T3A and T3B series (Coupland, 1990). For the T3A experiments, the author used a velocity of 5.4m/s and a turbulence intensity of 3.0%, and for the T3B experiments, a velocity of 9.4m/s and a turbulence intensity of 6.0%. For the test cases studied in this work, the meshes used are available in the TMR NASA Website (Rumsey, 2019).

Our results are confronted with the experiments mentioned before and the numerical results obtained in Langtry and Menter (2009) e Carnes and Coder (2022). For the T3A flat plate, the authors in Langtry and Menter (2009) used an inlet velocity of 5.4 m/s, a turbulence intensity, Tu_i, of 3.3%, a viscosity ratio, μ/μ_t, of 12.0. For the T3B case, the authors used an inlet velocity of 9.4 m/s, a Tu_i of 6.5%, and a μ/μ_t of 100.0. Carnes and Coder (2022) used for the T3A case a Tu_i of 5.855% and a μ/μ_t of 11.9. For the T3B test case, the authors used a Tu_i of 7.216% and a μ/μ_t of 99. The authors used a mesh with $271,425$ total points for both cases. In our c_f plots, the numerical results obtained in Langtry and Menter (2009) are named as Ref-1, and the numerical results presented in Carnes and Coder (2022) are called Ref-2. Our Reynolds numbers are calculated based on the inlet velocity given in the references. This strategy was made in order to obtain the same inlet velocity for a different Mach number. Our test cases and the reference freestream values are shown in Tables 1 and 2 for the T3A and the T3B test cases, respectively.

Table 1. Reference freestream values for the T3A zero pressure flat plate test cases.

Case	Re Number	Mach Number	Tu$_i$ (%)	μ_t/μ_{ref}	Mesh size (points)
Case A	3.6×10^5	0.15	3.3	12	26,578
Case B	3.6×10^5	0.15	5.855	11.9	26,578
Case C	3.6×10^5	0.15	3.3	12	419,650
Case D	3.6×10^5	0.15	5.855	11.9	419,650

Table 2. Reference freestream values for the T3B zero pressure flat plate test cases.

Case	Re Number	Mach Number	Tu$_i$ (%)	μ_t/μ_{ref}	mesh size (points)
Case E	6.27×10^6	0.15	6.5	100	419,650
Case F	1.32×10^6	0.15	6.5	100	419,650

Figure 1 shows the skin friction coefficient, c_f, for the T3A flat plate test cases. A comparison between the two meshes shows clearly the influence of the mesh size over the transition point location. The coarse mesh used for Cases A and B presents an early transition, while the fine mesh used for Cases C and D shows good agreement comparing with the references. For these two cases, we cannot observe an influence over the transition location when analyzing the two different physical input parameters. However, some influence over the transition location for these specific physical input parameters can be found in Righi *et al.* (2021). Figure 2 shows the numerical convergence history for Case A. For a matter of brevity, Case B presented the same convergence behavior and is not shown here. The four curves represent the normalized residues over the iterations for Case A considering the four compressible equations of the model, κ, ω, γ, and Re_{θ_t}. The curve for the turbulence dissipation, ω, equation presents the best numerical convergence history, while the curve for the intermittency, γ, equation does not present a good behavior. The curvers for the turbulence kinetic energy, κ,

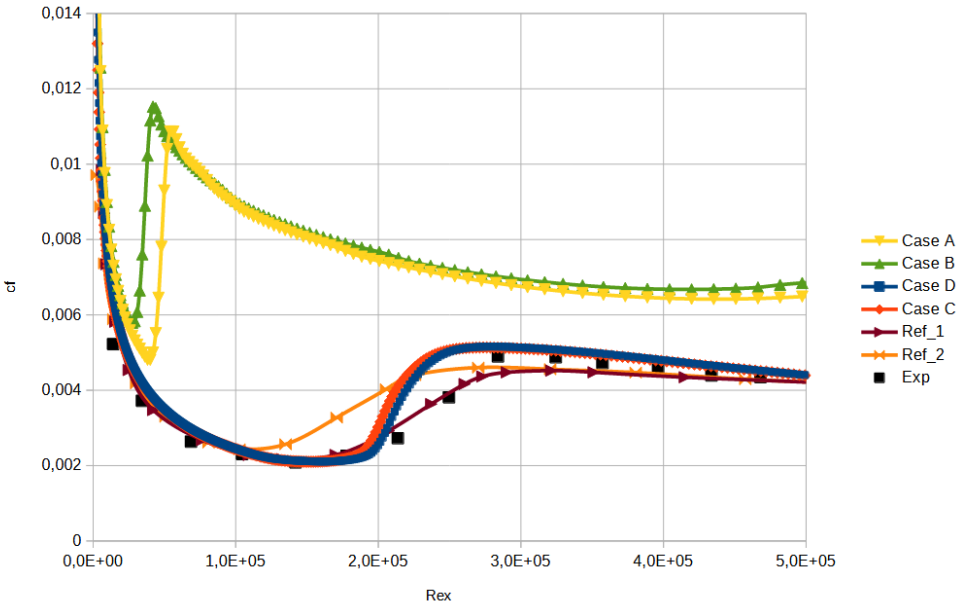

Figure 1. Skin friction coefficient, c_f, for the T3A zero pressure flat plate test cases.

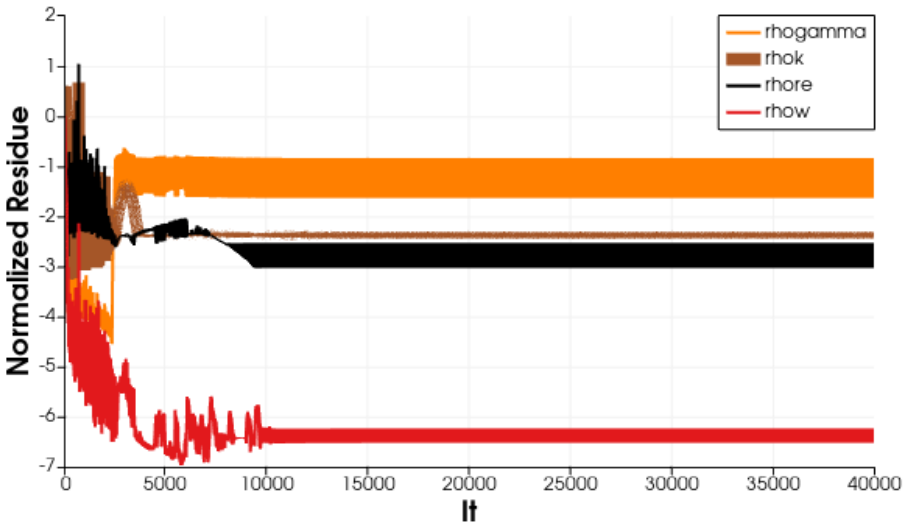

Figure 2. Numerical convergence history for Case A.

and the transition momentum-thickness Reynolds number, Re_{θ_t}, show a similar behavior. The residuals first rise followed by a decay in the convergence history until we observe a stall in the curves around $15,000$ iterations. We observe a high-frequency noise when the residuals stall. This is typical of transitional flow simulations and may be caused by the intermittency field oscillations in the near wall cells. Coder (2019) analyzes and explains the convergence behavior for the mean flow considering the same flat plate cases.

Figure 3 shows the numerical convergence history for Case C. For a matter of brevity, Case D presented the same convergence behavior and is not shown here. The four curves address the normalized residues over the iterations for Case C considering the four compressible equations of the model, κ, ω, γ, and Re_{θ_t}, as mentioned before. Comparison with Case A shows some differences in the residue convergence history in this case considering a fine mesh. The curve for the ω equation presents the best numerical convergence history. However, we observe an oscillatory behavior in this case. The oscillatory behavior in this case is developed around a constant average value, which is commonly observed in transitional flows. The same behavior is observed for the other equations, while the γ equation presents a lesser residue decay orders of magnitude and a less aggressive oscillatory behavior. The curvers for the κ and Re_{θ_t} show a similar behavior. Also, we observe that $15,000$ iterations are enough in order to obtain a converged solution.

Figure 4 presents the skin friction coefficient, c_f, for the T3B test cases. We observe good agreement comparing with the reference for the transition location, even though there is slightly earlier transition for Case E for which we

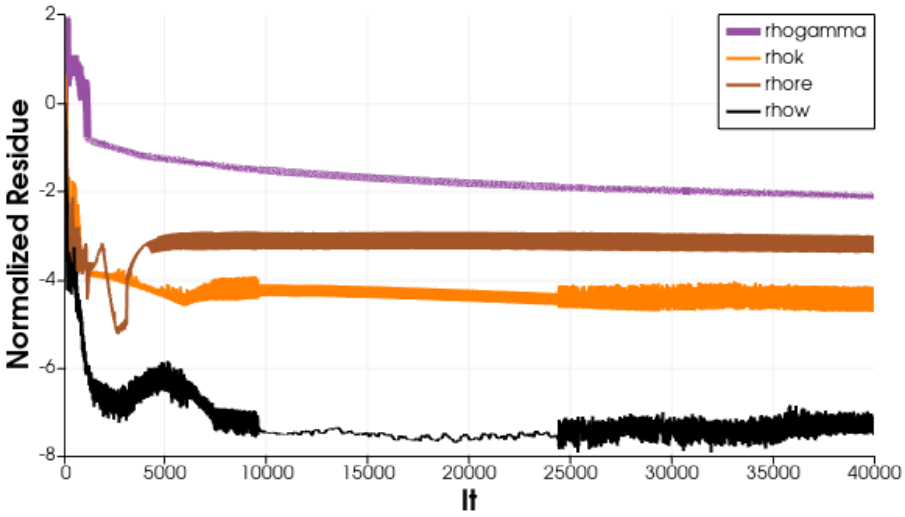

Figure 3. Numerical convergence history for Case C.

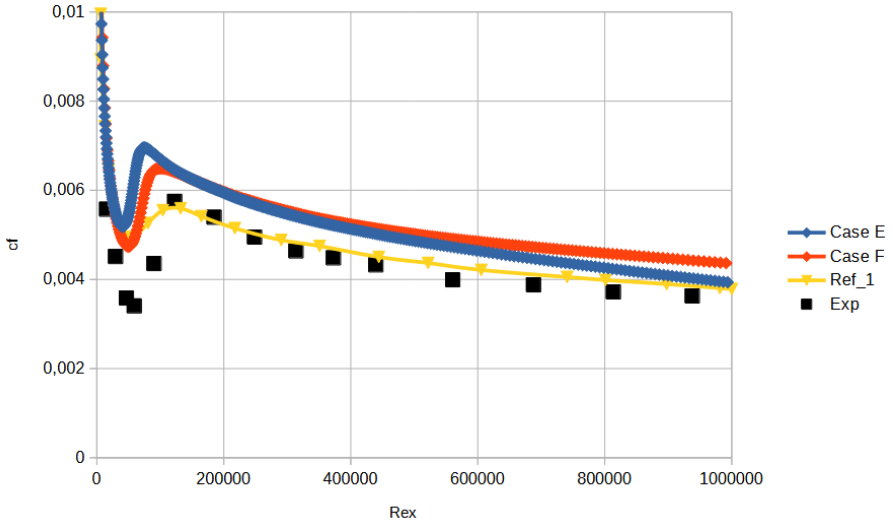

Figure 4. Skin friction coefficient, c_f, for the T3B zero pressure flat plate test cases.

considered a larger reference Reynolds number. Figure 5 shows the numerical convergence behavior over the iterations. As before, Case F presented similar convergence history and is not presented here. For the T3B test cases, the fine mesh was used in the simulations and we observed a similar behavior as for Cases C and D. The curve for ω presented the same oscillatory behavior with the best convergence history. There are two main differences in this case comparing with the cases before. First, the curve with less amount of decreased orders of magnitude is for the Re_{θ_t} equation followed by the γ equation, which are the two equations for the Langtry-Menter transition model. Second, the curves show a converged history behavior for the normalized residues over the iterations with $25,000$ iterations.

3.2 NLF(1)-0416 Airfoil

Four test cases are performed with the NLF(1)-0416 airfoil. The reference freestream parameters and mesh size for the tests are presented in Table 3. We confronted our numerical results with the numerical results published in Halila *et al.* (2019, 2022) and the experiments can be found in Somers (1981). The authors in Halila *et al.* (2019), which is called Ref-4 in our c_f plot, use a $Tu_i = 0.1\%$, a reference Reynolds number of 4 million, and a zero angle of attack. In Halila *et al.* (2022), which is refered as Ref-5 in our c_f plot, the authors used a $Tu_i = 0.15\%$, a reference Reynolds number of 4 million, a Mach number of 0.1, a zero angle of attack, and a computational mesh with $304,000$ cells. One of our goals was to study the transition front sensitivity with respect to the chord-based Reynolds number, and a validation of the model was presented in a previous work (Righi *et al.*, 2021) with the same value used by the references. For our studies, three meshes were used, one coarse, one fine and one super fine for different reference values. All three meshes were developed by the research group and Fig. 6 presents an example for the NLF(1)-0416 mesh used in the present work.

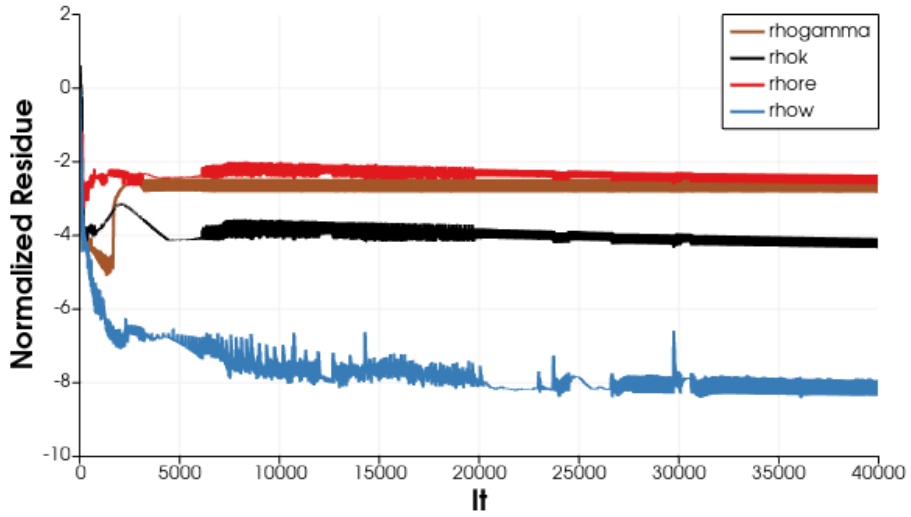

Figure 5. Numerical convergence history for Case E.

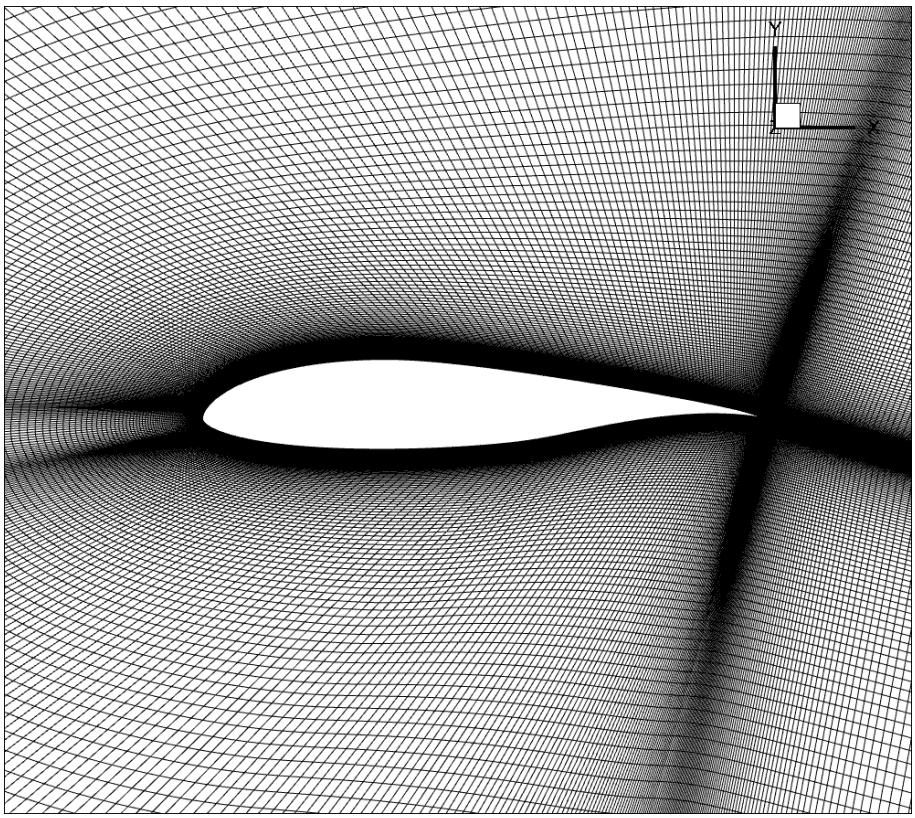

Figure 6. Example of the NLF(1)-0416 mesh used in the present work.

Table 3. Reference freestream values for the NLF(1)-0416 airfoil test cases.

Case	Re Number	Mach Number	Tu$_i$ (%)	μ_t/μ_{ref}	Mesh size (cells)
Case I	2.5×10^6	0.15	0.1	10.0	270,000
Case J	2.5×10^6	0.15	0.03	10.0	270,000
Case K	2.5×10^6	0.15	0.1	10	151,000
Case L	2.5×10^6	0.15	0.1	10	605,000

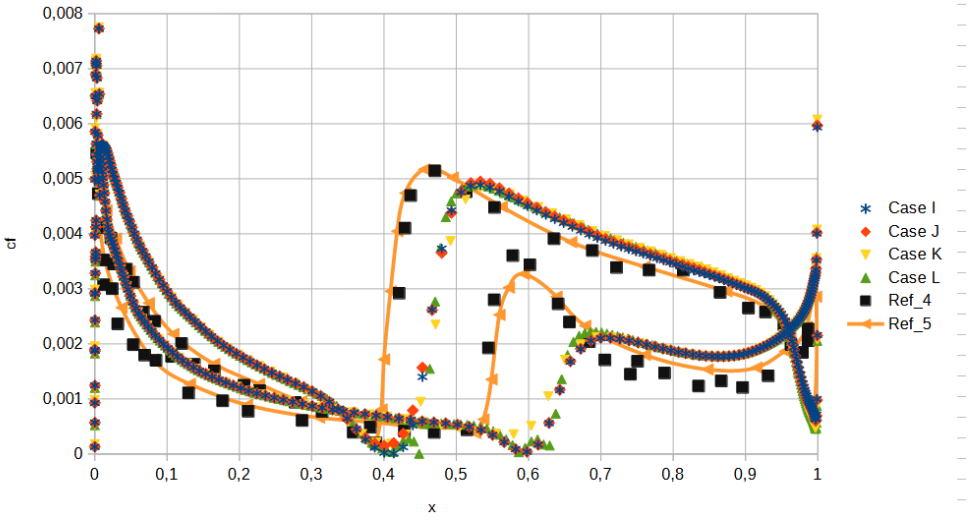

Figure 7. Skin friction coefficient, c_f, for the NLF(1)-0416 airfoil.

Figure 7 shows the skin friction coefficient, c_f, for the test cases mentioned before. Confronting with the reference, we observed a transition location in good agreement for the upper side, however, a late prediction for the transition location on the lower side of the airfoil. Also, the c_f curves are exactly the same for all the four test cases presented here. The simulations did not show any sensitivity in the c_f curves for different meshes or different physical reference parameters.

Figure 8 shows the numerical convergence history for Case J. For a matter of brevity, Case I presented the same convergence behavior and it is not presented here. The normalized residues over the iterations for the four equations show an oscillatory behavior. The best numerical convergence history is for the ω equation while the other three equations present similar behaviors. A number of $15,000$ iterations is enough for this case. The results for Case J are obtained using the fine mesh with $Tu_i = 0.03$, which is the smallest value studied here for the turbulence intensity. In this case, the residuals present an oscillatory behavior around a middle value for the four equations even after the residuals stall and such behavior is not observed for any other case studied here. After the solution stalls, the converged solution leads to a lift coefficient of $c_l = 0.48$ and a drag coefficient of $c_d = 0.006$.

Figure 9 presents the numerical convergence history for Case K using the coarse mesh. A number of $10,000$ iterations are enough to obtain a converged solution for engineering convergence strategy leading to a $c_l = 0.478$ and $c_d = 0.006$. The residuals do not show an oscillatory behavior when the solution is converged. One explanation for this may be the mesh, which is coarse and the effects in the solution for the other cases are not felt here. Still, the best convergence for the normalized residue is for the ω equation. The other equation for the SST turbulence model and the two equations for the Langtry-Menter transition model present a similar behavior in this case. Figure 10 shows the numerical convergence history for Case L for the super fine mesh. We observed that around $10,000$ iterations are enough to obtain a converged solution leading the a $c_l = 0.478$ and a $c_d = 0.006$. The normalized residue behavior is similar to the behavior for Case J. However, the γ equation present high-frequency oscillations, unlike the other curves. This behavior is seen by the solution for the super fine mesh for the γ equation and may be explained by the oscillations in the near-wall intermittency values, as mentioned before.

Including the turbulence equations in the set of the meanflow increases the complexity of the nonlinear system. Furthermore, adding the transport equations for the transition model increases the system complexity even more. This scenario impacts directly the numerical behavior, due to large number of nonlinearities that compose the simulations (Halila *et al.*, 2022). We observe in the first iterations a decay in the residuals followed by a rise. In this early stage, the flow is laminar and the turbulent flow is developing. In the early interations, the transition front is located at some point downstream and then moves upstream until it settles (Halila *et al.*, 2022). For all cases, the aerodynamic coefficients presented are converged when the transition front settles, and for engineering convergence purposes, we can consider the solutions converged.

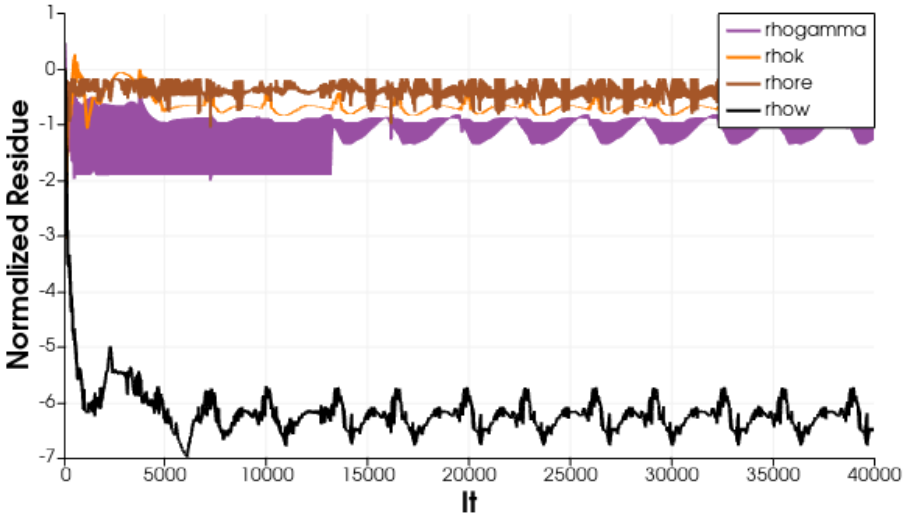

Figure 8. Numerical convergence history for Case J.

Figure 9. Numerical convergence history for Case K.

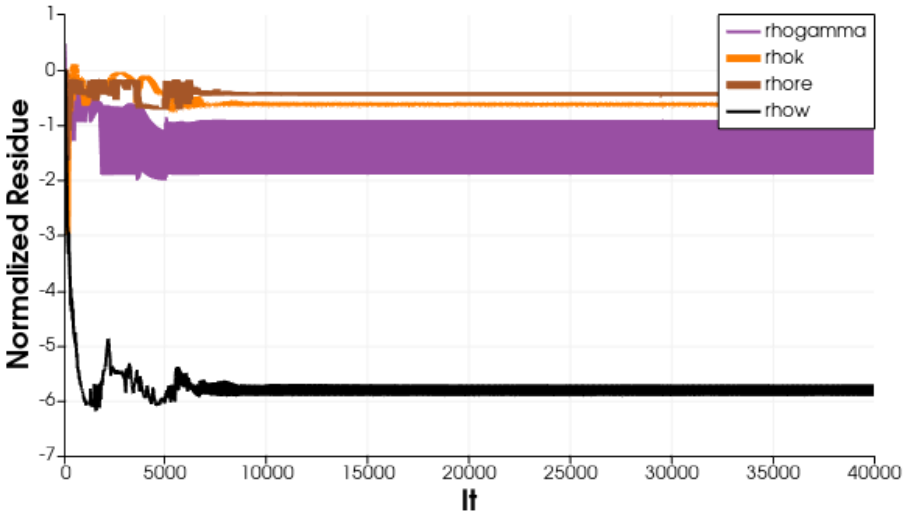

Figure 10. Numerical convergence history for Case L.

4. FINAL REMARKS

Modified RANS models considering transition effects have made possible to compute laminar and turbulent flow regions in the same CFD tool. The present study is concerned with the Langtry-Menter transition model coupled to the Shear Stress Transport (SST) turbulence model, which are implemented in an in-house CFD code with a Newton-Krylov solver. The present study aims to observe the differences in the skin friction coefficient, c_f, curves for the transition location and the numerical convergence history for different mesh sizes and reference physical values. The work considers the flows over two geometries, a zero pressure gradient flat plate test case and the NFL(1)-0416 airfoil. The results have highlighted the changes on the transition location due to the mesh size or physical reference values.

Overall, we observed good agreement with the literature data for the flat plate test case for the transition location. The results for the NLF(1)-0416 airfoil present good agreement for the transition location for the upper side of the airfoil, but there is some mismatch for the transition location in the pressure side of the airfoil. Also, we observed similar results in the c_f curves for all test cases studied here.

The numerical convergence histories presented different behavior for the test cases. However, for all test cases addressed in the present work, the best behavior of the normalized residue curves was always for the turbulence dissipation, ω, equation from the SST model. The other three equations presented similar behavior for most of the cases, although the level of convergence is, typically, considerably lower than that achieve in the turbulence dissipation equation. The authors also observed that most convergence curves exhibit quite oscillatory patterns, which is typical of RANS modified models that include transition to turbulence effects. The RANS modified models present some difficulties that are observed in this work, for example, the high-frequency noise and the amount of decreased orders of magnitude observed in the numerical convergence history curves. Finally, we observed fairly large differences in the number of necessary iterations in order to achieve a converged solution considering the different set up and mesh size studied in this work.

5. ACKNOWLEDGEMENTS

The authors gratefully acknowledge the support provided by Fundação de Amparo à Pesquisa do Estado de São Paulo, FAPESP, through a doctoral scholarship for the first author under Grant No. 2021/00031-0. The authors also gratefully acknowledge the support for the present research provided by Connselho Nacional de Desenvolvimento Científico e Tecnológico, CNPq, under the Research Grant No. 309985/2013-7. The work is also supported by the computational resources of the Center for Mathematical Sciences Applied to Industry (CeMEAI), funded by FAPESP under the Research Grant No. 2013/07375-0. This study was financed in part by the Coordenação de Aperfeiçoamento de Pessoal de Nível Superior (CAPES) - Finance Code 001.

6. REFERENCES

Bigarella, E.D.V., 2007. *Advanced Turbulence Modelling for Complex Aerospace Applications*. Ph.D. thesis, Instituto Tecnológico de Aeronáutica, São José dos Campos, Brazil.

Bigarella, E.D.V. and Azevedo, J.L.F., 2009. "A unified implicit CFD approach for turbulent-flow aerospace-configurations simulations". In *Proceedings of the 47th AIAA Aerospace Sciences Meeting Including the New Horizons*

Forum and Aerospace Exposition. Orlando, FL.

Carnes, J.A. and Coder, J.G., 2022. "Benchmarking the Langtry-Menter transition model using OVERFLOW for AIAA Transition Modeling Workshop". In AIAA 2022-3680*, Proceedings of the 2022 AIAA Aviation Forum*. Chicago, IL. doi:10.2514/6.2022-3680.

Carvalho, L.M.M.O., 2018. *Numerical Study of Transitional Flows Over Aerospace Configurations*. Master's thesis, Instituto Tecnológico de Aeronáutica, São José dos Campos, Brasil.

Carvalho, L.M.M.O., da Silva, R.G. and Azevedo, J.L.F., 2018. "Numerical study of transitional flows over aerospace configurations". In AIAA 2018-4209*, Proceedings of the 2018 AIAA Applied Aerodynamics Conference, AIAA Aviation Forum*. Atlanta, GA. doi:10.2514/6.2018-4209.

Coder, J.G., 2018. "Standard test cases for transition model verification and validation in computational fluid dynamics". In AIAA 2018-0029*, Proceedings of the 2018 AIAA Aerospace Sciences Meeting, AIAA SciTech Forum*. Kissimmee, FL. doi:10.2514/6.2018-0029.

Coder, J.G., 2019. "Further Development of the Amplification Factor Transport Transition Model for Aerodynamic Flows". In AIAA 2019-0039*, Proceedings of the 2019 AIAA Aerospace Sciences Meeting, AIAA SciTech Forum*. San Diego, CA. doi:10.2514/6.2019-0039.

Coupland, 1990. "Flat plate transitional boundary layers". Http://cfd.mace.manchester.ac.uk/ercoftac/doku.php?id=cases.

Ghasemi, E., McEligot, D., Nolan, K., Crepeau, Siahpush, A., Budwig, R. and Tokuhiro, A., October, 2014. "Effects of adverse and favorable pressure gradients on entropy generation in a transitional boundary layer region under the influence of freestream turbulence". *International Journal of Heat and Mass Transfer*, Vol. 77, pp. 475–488. doi: https://doi.org/10.1016/j.ijheatmasstransfer.2014.05.028.

Halila, G.L.O., Bigarella, E.D.V., Antunes, A.P. and Azevedo, J.L.F., 2018. "An efficient setup for freestream turbulence on transition prediction over aerospace configurations". *Aerospace Science and Technology*, Vol. 81, October, pp. 259–271. doi:10.1016/j.ast.2018.08.013.

Halila, G.L.O., Bigarella, E.D.V. and Azevedo, J.L.F., 2016. "A numerical study on transitional flows using a correlation-based transition model". *Journal of Aircraft*, Vol. 53, No. 4, pp. 922–941. doi:10.2514/1.C033311.

Halila, G.L.O., Chen, G., Shi, Y., Fidkowski, K.J., Martins, J.R.R.A. and Mendonça, M., 2019. "High-Reynolds number transitional flow prediction using a coupled discontinuous-Galerkin RANS PSE framework". *Aerospace Science and Technology*, Vol. 91, August, pp. 321–336. doi:10.1016/j.ast.2019.05.018.

Halila, G.L.O., Yildirim, A., Mader, C.A., Fidkwoski, K.J. and Martins, J.R.R.A., 2022. "Linear stability-based smooth Reynolds-averaged Navier-Stokes transition model for aerodynamic flows". *AIAA Journal*, Vol. 60, No. 2, pp. 1077–1090.

Klebanoff, P.S., Tidstrom, K.D. and Sargent, L.M., 1962. "The three-dimensional nature of boundary layer instability". *Journal of Fluid Mechanics*, Vol. 12, No. 1, pp. 1–24.

Langtry, R.B. and Menter, F.R., 2009. "Correlation-based transition modeling for unstructured parallelized computational fluid dynamics codes". *AIAA Journal*, Vol. 47, No. 12, pp. 2894–2906.

Menter, F.R., 1994. "Two-equation eddy viscosity turbulence models for engineering applications". *AIAA Journal*, Vol. 32, No. 8, pp. 1598–1605.

Poll, D.I.A., 1978. "Some aspects of the flow near a swept attachment line with particular reference to boundary layer transition". College of Aeronautics TR 7805, College of Aeronautics, Cranfield, England, UK.

Righi, A.R.S., Carvalho, L.M.M.O., Halila, G.L.O. and Azevedo, J.L.F., 2021. "A numerical study on the effects of mesh refinament, artificial dissipation, and freestream turbulence on laminar-turbulent transition predictions". In *Proceedings of the 26th International Congress of Mechanical Engineering, COBEM-2021*. Virtual Congress, Brazil.

Roe, P.L., 1981. "Approximatte Riemann solvers, parameter vector, and difference schemes". *Journal of Computational Physics*, Vol. 43, No. 2, pp. 357–372.

Rumsey, C., 2019. "Turbulence modeling resource". Https://turbmodels.larc.nasa.gov/.

Rumsey, C.L. and Lee-Rausch, E.M., 2015. "NASA trapezoidal wing computations including transition and advanced turbulence modeling". *Journal of Aircraft*, Vol. 52, pp. 496–509.

Saric, W.S. and Dagenhart, J.R., 1999. "Crossflow stability and transition experiments in swept-wing flow". NASA TP-1999-209344, NASA.

Slotnick, J., Khodadoust, A., Alonso, J., Darmofal, D., Gropp, W., Lurie, E. and Mavriplis, D., 2014. "CFD vision 2030 study: A path to revolutionary computational aerosciences". NASA CR–2014-218178, NASA.

Somers, D.M., 1981. "Design and experimental results for a natural-laminar-flow airfoil for general aviation applications". Technical Report NASA TP-1681, National Aeronautics and Space Administration – NASA.

Spalart, P.R. and Allmaras, S.R., 1994. "A one-equation turbulence model for aerodynamic flows". *La Recherche Aerospatiale*, , No. 1, pp. 5–21.

7. RESPONSIBILITY NOTICE

The authors are solely responsible for the printed material included in this paper.